Distributions and sea-to-air fluxes of nitrous oxide in the South China Sea and the West Philippines Sea

Hsiao-Chun Tseng [a,b], Chen-Tung Arthur Chen [b,*], Alberto V. Borges [c], T. Angel DelValls [a], Chao-Ming Lai [d], Ting-Yu Chen [b]

[a] UNESCO UNITWIN/WiCop. Physical Chemistry Department. Faculty of Marine and Environmental Sciences. Polígono río San Pedro s/n, University of Cadiz, 11519 Puerto Real, Cadiz, Spain
[b] Department of Oceanography, National Sun Yat-sen University, Kaohsiung 804, Taiwan
[c] Université de Liège, Unité d'Océanographie Chimique, Institut de Physique (B5), B-4000, Belgium
[d] Departmentt of Agricultural Chemistry, National Taiwan University, Taipei 106, Taiwan

ABSTRACT

Approximately 600 water samples from the South China Sea (SCS) and 250 water samples from the West Philippines Sea (WPS) were collected during seven cruises from August 2003 to July 2007 to determine nitrous oxide (N_2O) distributions between the surface and a maximum depth of 4250 m. In the SCS, the average surface N_2O concentration exceeded the atmospheric equilibrium concentration (on average $132 \pm 23\%$); however in the WPS, the surface N_2O concentration was lower than the atmospheric equilibrium concentration (on average $90 \pm 22\%$). The N_2O concentration reached a maximum (~ 23 nmol L^{-1}) in the WPS at 800–1000 m, and (~ 28 nmol L^{-1}) at a shallower depth of around 600–800 m in the SCS, owing to vertical mixing and intensive upwelling in the SCS. In the SCS, the surface N_2O concentration was 7.59 ± 1.32 nmol L^{-1} and the calculated sea-to-air flux was 5.5 ± 3.9 µmol m^{-2} d^{-1}. The surface N_2O concentration in the WPS, 5.19 ± 1.26 nmol L^{-1}, was lower than that in the SCS. The WPS is a sink for N_2O and the calculated sea-to-air flux was -1.7 ± 3.9 µmol m^{-2} d^{-1}. The SCS emitted 19.3×10^6 mol d^{-1} N_2O to the atmosphere and exported 8.5×10^6 mol d^{-1} N_2O to the WPS during the wet season.

© 2016 Elsevier Ltd. All rights reserved.

1. Introduction

Nitrous oxide (N_2O) is a trace gas that strongly influences the climate and atmospheric chemistry. It is a long-lived and powerful greenhouse gas (Prather et al., 2012), ranking third in anthropogenic radiative forcing, only behind carbon dioxide (CO_2) and methane (CH_4) (Myhre et al., 2013). Additionally, N_2O has a global warming potential in a 100-year time frame (GWP_{100}) that is 298 times that of CO_2 (IPCC, 2013). Atmospheric concentrations of N_2O have risen from 270 ± 7 ppb in 1750–324.2 ± 0.1 ppb in 2011 (IPCC, 2013). The gas also affects the climate by interacting with the stratospheric ozone (Crutzen, 1974; Nevison and Holland, 1997; Prather et al., 2001) as the N_2O in the stratosphere is an important precursor of nitric oxide (NO) radicals, which are involved in the depletion of the atmospheric ozone (Crutzen, 1970; Ravishankara, et al., 2009). Since 2011, N_2O has become the dominant ozone-depleting substance on account of the decrease in the impact of

dichlorodifluoromethane (CFC-12) after the implementation of the Montreal Protocol and amendments (Ravishankara et al., 2009).

Natural sources of N_2O include oceans, sediments, inland waters, and terrestrial soils. However, global inventories of these sources are still fairly uncertain. According to the Fifth Assessment Report of the Intergovernmental Panel on Climate Change (IPCC 5AR), the oceans are significant sources of the atmospheric N_2O, and account for approximately one-third of global natural emissions and one-fifth of total (natural and anthropogenic) emissions. Nevison et al. (1995) computed a global ocean source of 4 Tg N yr^{-1}, with a large range of uncertainty from 1.2 to 6.8 Tg N yr^{-1} based on 60,000 at-sea measurements. Model-derived estimates also vary widely, between 1.7 and 8 Tg N yr^{-1} (Nevison et al., 2003; Suntharalingam and Sarmiento, 2000). Recently, Manizza et al. (2012) used a large-scale ocean general circulation model that was coupled with a biogeochemical model to quantify mean ocean emissions at 4.5 TgN yr^{-1}, while Saikawa et al. (2014) estimated an oceanic N_2O source with a flux of between 3.6 and 5.2 TgN yr^{-1}, based on a global atmospheric inversion model. These large uncertainties arise from too few observations and poor

* Corresponding author.
E-mail address: ctchen@mail.nsysu.edu.tw (C.-T. Chen).

knowledge of mechanisms of N_2O formation, reflecting a general lack of understanding of key aspects of the oceanic nitrogen cycle (Gruber and Galloway, 2008; Zehr and Ward, 2002), and of N_2O in particular (e.g., Bange et al., 2009; Freing et al., 2012; Zamora et al., 2012, among others).

Most N_2O in oceanic environments is formed from NH_2OH as a byproduct of nitrification ($NH_4^+ \rightarrow NH_2OH \rightarrow NO_2^- \rightarrow NO_3^-$) and as an intermediate product during denitrification ($NO_3^- \rightarrow NO_2^- \rightarrow N_2O \rightarrow N_2$). During autotrophic nitrification N_2O can be formed by $NH_4^+ \rightarrow NH_2OH (\rightarrow NO) \rightarrow NO_2^-$ either via the pathways $NH_2OH \rightarrow N_2O$ and $NO \rightarrow N_2O$ (Arp and Stein, 2003; Stein and Yung, 2003) or via the pathway $NO_2^- \rightarrow NO \rightarrow N_2O$ (the latter is part of the so-called nitrifier-denitrification process) (Stein and Yung, 2003; Wrage et al., 2001). Nitrification is believed to be the main contributor to the production of N_2O in seawater (Najjar, 1992; Bange and Andreae, 1999; Freing et al., 2012). Denitrification occurs under low oxygen ($< 6 \mu mol L^{-1}$) to anoxic conditions (Nevison et al., 2003). Denitrification produces and consumes N_2O in oxygen minimum zones and the net result is that oxygen minimum zones have some of the highest N_2O concentrations in the ocean (LaMontagne et al., 2003; Naqvi et al., 2010; Zamora et al., 2012; Arévalo-Martínez et al., 2015). In the water column with low oxygen concentrations and in sediments or inside suspended particles, nitrification and denitrification can occur simultaneously and are often closely coupled (Seitzinger, 1988; Ward et al., 1989; Capone, 1991; Middelburg et al., 1996; Barnes and Owens, 1998; Naqvi et al., 1998; Robinson et al., 1998; Usui et al., 2001; Nevison et al., 2003; Codispoti et al., 2005; Bange, 2008). The yield of N_2O from both processes is highly dependent on the concentration of dissolved oxygen (Goreau et al., 1980; de Bie et al., 2002; Naqvi et al., 2010).

Few investigations of N_2O in the South China Sea (SCS) have been published, and these have only considered the northern part (Xu et al., 2006; Zheng et al., 2009; Han et al., 2013). Almost no data on N_2O in the West Philippines Sea (WPS) are available. This paper presents the spatial and vertical distributions of N_2O in the water columns of the SCS and the WPS as well as the sea-to-air fluxes. The differences between these seas and the influencing factors are discussed. Additionally, previous research in the SCS calculated the excess N_2O (ΔN_2O) concentration by using "the contemporary atmospheric mole fraction" throughout the water column. This study for the first time calculates the ΔN_2O by using "the initial atmospheric mole fraction" to reduce the uncertainty of ΔN_2O.

2. Study area

The SCS is the largest marginal sea in the world with an area of $3.5 \times 10^6 km^2$ and an average depth of 1350 m. At the southern edge of the SCS lies the Sunda Shelf, which has a mean depth of around 50 m and is connected to the Straits of Malacca. The Mindoro Strait connects the eastern SCS with the Sulu Sea and the Taiwan Strait connects the northern SCS with the East China Sea. The northeastern SCS is connected with the WPS via the Luzon Strait, which has the deepest sill of any that connects the SCS with any adjacent bodies of water. As the Luzon Strait is 2200 m deep, the surface and intermediate waters are exchanged freely between the SCS and the WPS. Whereas waters that are deeper than 2200 m in the WPS cannot enter the SCS. Consequently, waters deeper than 2200 m in the SCS are relatively homogeneous, with hydrochemical properties that are similar to those of the water at 2200 m in the WPS (Chen et al., 2006).

The WPS is located in the western part of the North Pacific with an average depth of around 5500 m, and it is bordered by the Japanese islands of Honshu, Shikoku, and Kyushu to the north, the Ryukyu Islands to the northwest, Taiwan to the west, the Philippine archipelago to the southwest, and the Izu-Ogasawara Ridge and the Mariana Ridge to the east. The Kyushu-Palau Ridge (at a longitude of around 135°E) separates the West Mariana Basin from the WPS. This study focuses on the region between 120.5°E and 126.5°E and between 21°N and 26°N, where the WPS connects with the SCS and a significant quantity of water is frequently exchanged.

The Asian monsoon dominates climatic variations at the sea-air interface of the SCS. The southwest monsoon season runs from May to October and brings extensive precipitation; it is the wet season in Southeast Asia. The northeast monsoon season runs from November to April and is characterized by high wind speeds (Han, 1998). The seven cruises herein were all conducted during the wet season.

3. Materials and methods

3.1. Sample collections

Samples were taken during five cruises on board R/V Ocean Researchers I and III in the SCS (Fig. 1a; Table 1), designated ORIII-896 (August 2003), ORI-695 (September 2003), ORIII-983 (July 2004), ORI-802 (July 2006), and ORI-837 (July 2007).

Samples were collected close to the south of the Taiwan Strait, which is located in the northeastern part of the SCS, during the cruises in August 2003 (ORIII-896) and July 2004 (ORIII-983). ORI-695 was conducted near the Pearl River estuary and was influenced by the summer estuarine plume (Gan et al., 2009; Cao et al., 2011; Han et al., 2012; Zhai et al., 2013; Bai et al., 2015). The Pearl River (Zhujiang) is the 13th largest river in the world (Yin et al., 2004) and the second largest river in China (after the Yangtze River) with a water discharge of $326 \times 10^9 m^3$ annually; it is also the second largest river (after the Mekong River) that enters the SCS (Chen et al., 2008).

In July 2006 (ORI-802), samples were taken on the Sunda Shelf and on the continental slope, where the depth increases sharply. From July 16–31 of 2007 (ORI-837), surface water samples were taken from the Luzon Strait and along the western coast of Luzon Island, Palawan Island, and the northwestern coast of Borneo Island; profile water samples were taken at various depths from the eastern part of the SCS to the southern part of the SCS.

Samples were obtained from the WPS during three of the cruises (Fig. 1b; Table 1). Profile water samples were taken at various depths on ORI-725 (August 2004) and ORIII-1149 (May 2006). These two cruises were conducted along 22°N from 120.5°E to 126.5°E in August 2004 and from 120.5°E to 124°E in May 2006, respectively. Surface water samples were taken from the northeastern coast of Taiwan to the Luzon Strait on ORI-725 (August 2004) and ORI-837 (July 2007).

Water samples were collected from various areas and depths using a Rosette sampler that was fitted with 5 L or 10 L Niskin bottles along with a conductivity–temperature–depth (CTD) probe (Sea-Bird 911, USA). Saturated $HgCl_2$ was added to all samples to inhibit microbial activity, excluding those that were used to measure salinity. Temperature data were obtained from the CTD profiles, whereas the salinity values that were used in the analysis were determined from discrete AUTOSAL measurements.

Water samples that were used to measure N_2O concentration were collected in 120 ml dark glass bottles. The bottles were rinsed three times using the sampled water. After one fold of bottle volume was allowed to overflow the bottle, 10 ml of the water sample was withdrawn from the bottle to leave an air space and 0.5 ml saturated $HgCl_2$ was then added. The sample bottles were then immediately sealed with a butyl rubber stopper and an
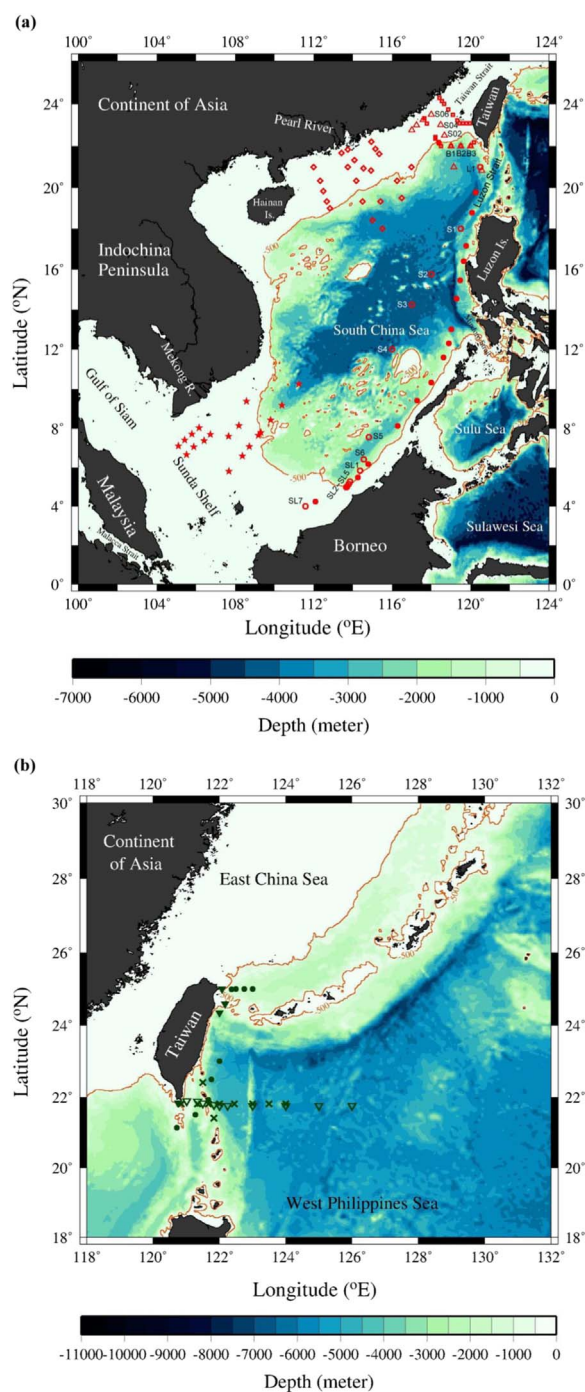
Fig. 1. Study area and station locations: (a) South China Sea stations. (surface sampling stations, •: ORI-837 (Jul. 2007); profile sampling stations, △: ORIII-896 (Aug. 2003), ◇: ORI-695 (Sep. 2003), □: ORIII-983 (Jul. 2004), ☆: ORI-802 (Jul. 2006), ○: ORI-837 (Jul. 2007); (b) West Philippines Sea stations. (surface sampling stations, ▼: ORI-725 (Aug. 2004), •: ORI-837 (Jul. 2007) -Stn. A-D;1–5; profile sampling stations, ▽: ORI-725 (Aug. 2004), ×: ORIII-1149 (May 2006)).

aluminum cap. The samples were stored in a dark box at 4 °C. All water samples were transferred to a laboratory and analyzed within three months of collection.

3.2. Chemical analysis

The salinity of the water samples was determined by measuring the conductivity using an AUTOSAL salinometer (Guildline Instruments), which was calibrated using the standard seawater

(batch no. P141) from the International Association for the Physical Sciences of the Oceans (IAPSO). The precision of the salinity measurements was ± 0.003. Chlorophyll a samples were collected by filtration through a 0.45 μm diameter Millipore polycarbonate filter. A Turner Designs model 10-AU fluorometer (Varian Eclipse) was utilized to measure chlorophyll a concentration following extraction by 90% acetone (Strickland and Parsons, 1972) with a precision of $\pm 5\%$. Dissolved oxygen (DO) concentration was measured by the direct spectrophotometry (Pai et al., 1993) with a precision of about $\pm 0.32\%$ at the 190 μmol L^{-1} level. The apparent oxygen utilization (AOU) was calculated using the oxygen solubility equation of Chen (1981), as a function of salinity and temperature. Nitrate (NO_3^-) plus nitrite (NO_2^-) concentration was measured by the pink azo dye method (Strickland and Parsons, 1972) using a flow injection analyzer and an online Cd coil. The precision of this method was around $\pm 1\%$ at 35 μmol L^{-1}, and $\pm 3\%$ at 1 μmol L^{-1}. The NO_2^- concentration was also obtained by the pink azo dye method (Strickland and Parsons, 1972; Pai et al., 1990) using a flow injection analyzer, yielding a precision of ± 0.02 μmol L^{-1}.

The concentration of dissolved N_2O was estimated using the modified headspace equilibrium method (Johnson et al., 1990) with gas chromatographs (GC; Varian 3600 and 3800) that were equipped with electron capture detectors (ECD). The samples were placed in a water bath at a constant temperature of 25 °C, and allowed to equilibrate for at least three hours. Two ml of the gas from the headspace was injected into the GC. The GC-ECD had a 3.6 m $\times$ 1/8 in. stainless steel column, which was filled with 80/100 mesh Porapak Q. The ECD was calibrated with pure N_2 (Jing-Shang, Taiwan) and two commercial gas mixtures with an N_2O mixing ratio of 1.0 ppmv (Scott Specialty Gases, U.S.A.) and 2.5 ppmv (All-Win, Taiwan). The precision of the repeated routine analysis of water samples was approximately $\pm 5\%$ of the concentration of N_2O. To acquire the calibration curve, airtight bags were used to mix pure N_2 with two standard gases to reach N_2O concentrations of 0, 0.25, 0.5, 0.75, 1, 1.5, 2, and 2.5 ppmv for calibration of the GC-ECD. Each calibration curve had a $R^2 > 0.999$. The N_2O concentration in the headspace of our samples were measured and followed the modified headspace equilibrium method (Johnson et al., 1990), as follows:

$$C_{seawater} = [C_{headspace\ gas}\left((\beta/24.3)RT + V_{gas}/V_{seawater}\right)$$
$$- C_{air} * V_{gas}/V_{seawater}]/24.3$$

Where $C_{seawater}$ is N_2O concentration in the seawater; $C_{headspace\ gas}$ is N_2O concentration in the headspace gas; β is Bunsen solubility of N_2O; 24.3 is the molar volume of N_2O in L mol^{-1}; R is the gas constant in L atm mol^{-1} K^{-1}; T is in K; V_{gas} is the volume of the gas phase; $V_{seawater}$ is the volume of the liquid phase; and C_{air} is atmospheric N_2O concentration. The calibration curve was used to calculate the N_2O concentration in the headspace and then the N_2O concentration in the seawater was calculated according to the above equation. The highest N_2O concentrations of the headspace gas was around 2.5 ppm. The N_2O concentrations of the headspace gas fitted in our calibration curve.

3.3. Saturation ratio

The concentrations of the N_2O in the water samples were obtained from those that were measured in the headspace by subtracting the influence of atmospheric N_2O and using Bunsen coefficients to calculate the equilibrium solubilities, as described by Weiss and Price, (1980).

The atmospheric N_2O concentrations were taken from the NOAA/ESRL in situ program (http://www.esrl.noaa.gov/gmd). The annual average atmospheric N_2O concentrations at Mauna Loa

Table 1
Seven research cruises were conducted in the SCS and the WPS.

Study area		Date	Cruise	Station	Surface N$_2$O (nM)	
					Range	Average
SCS	The northeastern SCS	Aug. 2003	ORIII-896	11	7.72–14.20	10.33 ± 1.93
	Pearl River estuary	Sep. 2003	ORI-695	22	6.30–8.29	7.45 ± 0.55
	The northeastern SCS	July 2004	ORIII-983	22	6.74–10.30	7.96 ± 0.84
	The southwestern SCS	Jul. 2006	ORI-802	20	5.52–7.84	6.84 ± 0.60
	The eastern and southern SCS	Jul. 2007	ORI-837	31	6.10–8.14	6.91 ± 0.42
WPS	along 22°N from 121°E to126°E	Aug. 2004	ORI-725	24	3.82–5.52	4.65 ± 0.39
	along 22°N from 121°E to124°E	May. 2006	ORIII-1149	11	3.19–5.84	4.70 ± 0.98
	From northeastern coast of Taiwan to the Luzon Strait (surface water only)	Jul. 2007	ORI-837	9	6.22–8.19	7.31 ± 0.71

(Hawaii, United States station) in the years 2003–2007 were 318.26 ppbv, 318.96 ppbv, 319.75 ppbv, 320.48 ppbv, and 321.35 ppbv, respectively.

Saturation, expressed in %, was calculated using $R=(C_{obs}/C_{eq})*$ 100 where C_{obs} represents the observed concentration of the gas that was dissolved in the water, and C_{eq} is the expected equilibrium water concentration, computed using the Henry's Law.

3.4. Excess N$_2$O (ΔN$_2$O)

The excess N$_2$O (ΔN$_2$O) concentration was calculated as the difference between the calculated N$_2$O equilibrium concentration and the observed N$_2$O concentration as follows:

$$\Delta N_2O\left(nmolL^{-1}\right) = N_2O\left(observed\right) – N_2O\left(equilibrium\right).$$

To calculate the N$_2$O equilibrium concentration, different atmospheric mole fractions were used for different water layers. Between the mixed layer and the atmosphere, N$_2$O exchanges occurred within three weeks or so (Najjar, 1992); thus, we calculated N$_2$O in the mixed layer using the actual atmospheric N$_2$O value. That is, the ΔN$_2$O in the surface water layer (0–350 m) was calculated using the actual atmospheric N$_2$O concentration of 318–321 ppb for 2003–2007. Below the thermocline, in the absence of exchange with the atmosphere, the calculated N$_2$O equilibrium concentrations depend on the atmospheric N$_2$O mole fraction at the time of deep-water formation. However, the exact atmospheric mole fraction of N$_2$O during deep-water formation is unknown because of uncertainty in the determined age of water masses (Walter et al., 2006). According to England (1995) modeling data, the intermediate water (755 m) and the deep water (1622 m) in the western North Pacific Ocean are approximately 500 and 900 years old. The radiocarbon observations that were made by Gebbie and Huybers (2012) indicated that the Pacific Deep Water (PDW) is 1200–1500 years old. Therefore, ΔN$_2$O in the intermediate water layer (350–1350 m) and the deep water layer (1350–2200 m) of the WPS was calculated using the tropospheric preindustrial value of 270 ppb (Fluckiger, et al., 1999); for depths > 2200 m, an atmospheric value of 260 ppb (MacFarling Meure et al., 2006) was used.

Chen and Huang (1995), Chen et al. (2015) reported that waters in the SCS exchange rapidly and horizontally with the WPS so the intermediate and deep waters are essentially of the same age as corresponding waters in the WPS. The deep WPS water at around 2200 m flows across the deep sill (Chen et al., 2001) into the SCS and has become the deep water and the bottom water of the SCS (Nitani, 1972; Liu and Liu, 1988; Chen et al., 2001). Therefore, the waters at around 2200 m and deeper in the SCS are of similar age as the water at 2200 m in the WPS. Consequently, an atmospheric value of 270 ppb was used to calculate the ΔN$_2$O for the water depth greater than 350 m in the SCS.

3.5. Fluxes

Fluxes of N$_2$O across the air-water interface were estimated using $F=k(C_w-\beta C_a)$ where C_w represents the concentration of dissolved gas in the water (mol L^{-1}); β is the Bunsen solubility, C_a is the atmospheric gas concentration, and k (cm h^{-1}) is the gas exchange coefficient. The value of k is a specific function of the property of the gas, the temperature T (°C) and the wind speed u (m s^{-1}). In the previous research, k has commonly been calculated using the linear k/wind speed relationship that was established by Liss and Merlivat (1986) (LM86) or the quadratic k/wind speed relationship that was established by Wanninkhof, (1992) (W92). Wanninkhof, (2014) updated the frequently used method of Wanninkhof, (1992), and a new k was calculated. The updated relationship is given by $k=0.251\,u^2\,(Sc/660)^{-0.5}$, where k is the gas transfer velocity; u is the mean wind speed, and Sc is the Schmidt number, which is the kinematic viscosity of water divided by the molecular diffusion coefficient of the gas. A positive flux indicates the gas transfer from the water to the atmosphere.

Wind speeds at 10 m above the surface were obtained from the National Aeronautics and Space Administration (NASA) QuikSCAT satellite platform (https://winds.jpl.nasa.gov/missions/quikscat/). The average monthly wind speed was used to estimate the sea-to-air flux. The seawater fluxes from the SCS to the WPS were taken from Chen et al. (2001). The principle of conservation of water masses requires that the flow of water into the SCS be balanced by the outflow of water.

4. Results and discussion

4.1. West Philippines Sea

The average surface N$_2$O concentration in the WPS in the wet season was 5.19 ± 1.26 nmol L^{-1} (90 ± 22% saturation; n=43). In the WPS, the N$_2$O (Fig. 2a) concentration gradually increased with the depth up to 1000 m, reaching a maximum of approximately 23 nmol L^{-1} at 800–1000 m, coinciding with a DO minimum (Fig. 2b). The N$_2$O concentration gradually decreased with depth beyond 1000 m because seawater at depths of greater than 1000 m in the WPS reflects the N$_2$O distribution of the Pacific Deep Water (PDW), which has a low N$_2$O concentration. According to Usui et al. (1998), Bange and Andreae (1999), the N$_2$O concentration at depths of 3000–5000 m in the North Pacific is only around 17.5–22 nmol L^{-1}.

4.2. South China Sea

The surface N$_2$O concentration in the wet season in the SCS was 7.59 ± 1.32 nmol L^{-1} (132 ± 23% saturation; n=105). The N$_2$O
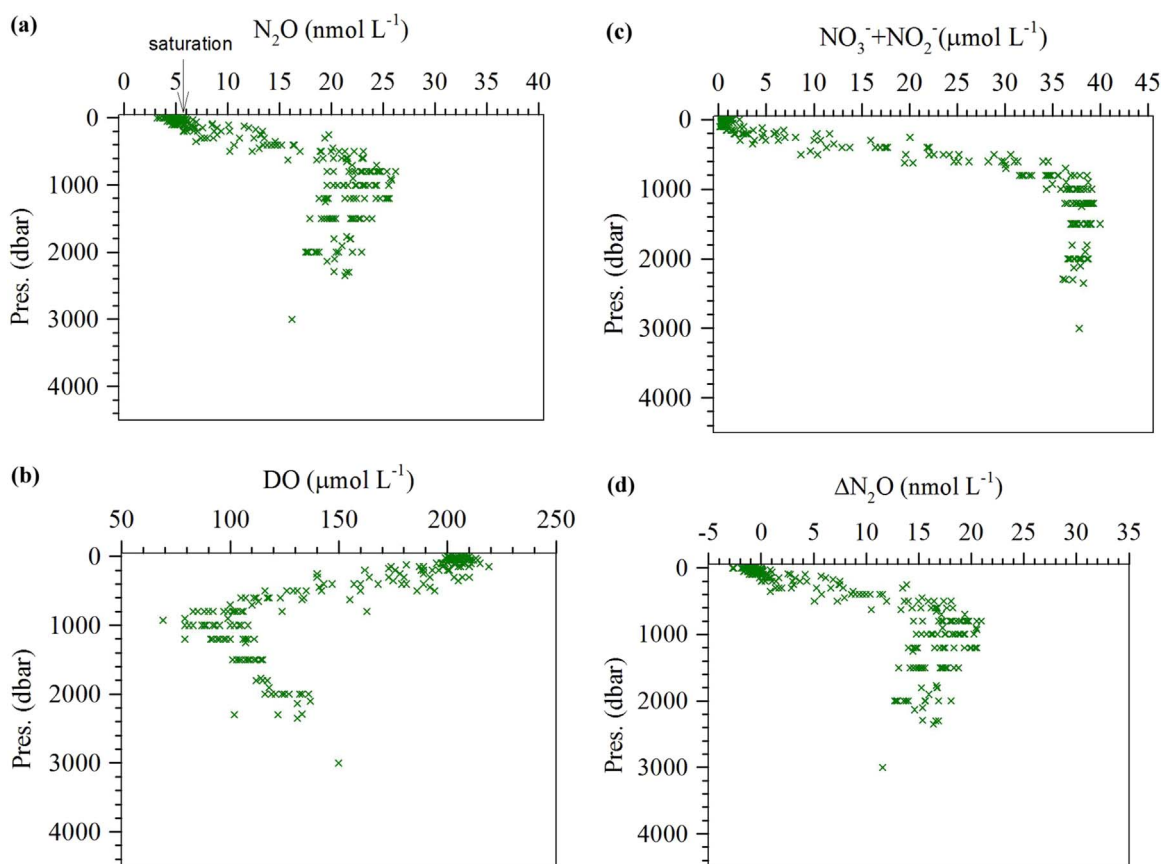
(a)

(b)

(c)

(d)

Fig. 2. Vertical distributions of (a) N_2O (nmol L^{-1}); (b) DO (μmol L^{-1}); (c) $NO_3^- + NO_2^-$ (μmol L^{-1}); (d) ΔN_2O (nmol L^{-1}) in the West Philippines Sea, obtained at 44 stations during three cruises between August 2004 and July 2007.

concentration in the water column of the SCS notably exceeds that in the WPS, and the SCS has a shallower N_2O maximum (Fig. 3a) at approximately 600–800 m compared with the 800–1000 m in the WPS. This is due to the upwelling in the SCS. In both the SCS and the WPS, the N_2O maxima (Figs. 2a and 3a) are at the depths where DO is at a minimum (Figs. 2b and 3b). The surface and intermediate waters are exchanged freely between the SCS and the WPS, and the deep water below 1350 m flows into the SCS from the WPS (Chen et al., 2001). However, waters at depths of greater than 2200 m in the WPS, including the Pacific Deep Water and the Antarctic Bottom Water, cannot enter the SCS (Chen et al., 2001, 2006). The intermediate and deep SCS waters above 2200 m mix with the WPS water, which has a lower N_2O concentration, so the N_2O concentration gradually decreases with increasing depth beyond the N_2O maximum but remains constant at depths in excess of 2200 m.

In the SCS, some sampling stations close to the continental slope have high N_2O concentrations ($N_2O > 32$ nmol L^{-1}; Fig. 3a) at around 400–1000 m. Fig. 4 shows the cross-section in the northeastern SCS in 2003 (ORIII-896) and Fig. 5 presents the cross-section between the eastern and the southern SCS in 2007 (ORI-837). The water column of the sections were well stratified in both temperature and salinity in the summer (Figs. 4a, b, 5a, and b). The DO concentrations decreased from the surface layer to the DO minima (Figs. 4c and 5c) while N_2O concentrations increased with the depth to the N_2O maxima at approximately 600–800 m (Figs. 4d and 5d). Figs. 4d and 5d show that sampling stations close to the continental slope have high N_2O concentrations at around 400–1000 m. Similarly, Zhang et al. (2008) measured high concentrations of N_2O in the bottom waters of the continental slope in the East China Sea, which may have been related to the production

and emission of N_2O from the organic-rich sediments or re-suspended particles (Zhu et al., 2006). Lin et al. (1992) found a layer with a high particle concentration immediately above the sediments on the continental slope, probably as a result of the cross-shelf transport. Walsh et al. (1985) suggested that lateral particle transport in the water column has an important role in determining the final fate for the organic particle. Therefore, these high N_2O concentrations are assumed herein to have been produced from organic particles on the continental slope close to the sampling stations. High CH_4 concentrations were also observed at the sampling stations close to the continental slope (Tseng et al., submitted).

4.3. Comparison of N_2O distributions in the SCS and WPS

The average surface N_2O concentration during the wet season in the SCS was about 30% higher than that in the WPS. There are many rivers flowing into the SCS, which discharge not only rich nutrients but also high concentrations of N_2O (Chen et al., 2008). Fig. 6 presents the surface distribution of salinity and N_2O near the Pearl River estuary in 2003. Higher N_2O concentrations with lower salinities occurred near the estuaries (Fig. 6). This result indicates that the high surface N_2O concentrations near the Pearl River estuary was caused by fresh water inputs. Additionally, upwelling often occurs in the SCS (Zheng and Tang, 2007; Han et al., 2013), bringing nutrients and high concentrations of N_2O from greater depths to the surface waters. Furthermore, increasing nutrient contents and subsequent phytoplankton blooms (Zheng and Tang, 2007; Herbeck et al., 2011) may also influence the production and emission of N_2O (Naik et al., 2008; Walker et al., 2010) in the SCS. Figs. 2c and 3c show the distributions of $NO_3^- + NO_2^-$ in the
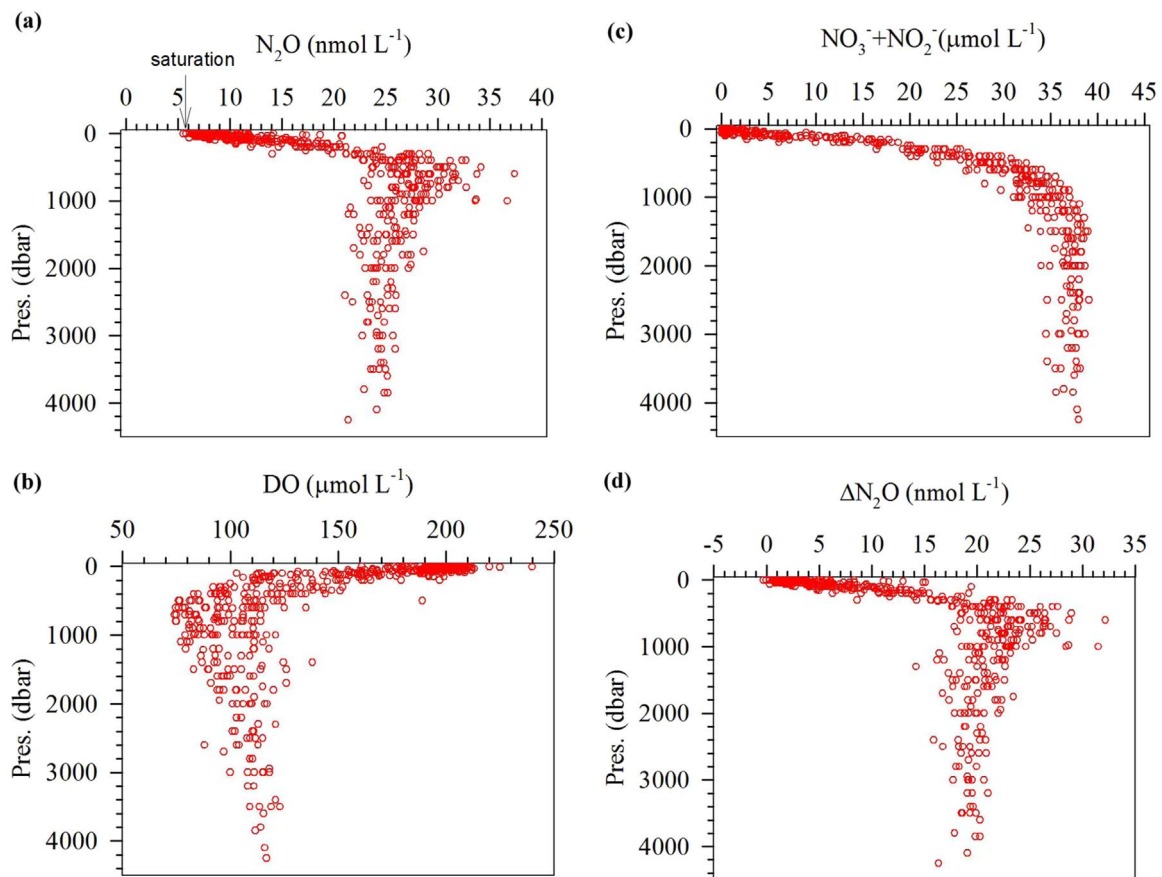
Fig. 3. Vertical distributions of (a) N_2O (nmol L^{-1}); (b) DO (μmol L^{-1}); (c) $NO_3^- + NO_2^-$ (μmol L^{-1}); (d) ΔN_2O (nmol L^{-1}) in the South China Sea, obtained at 106 stations during five cruises between August 2003 and July 2007.

WPS and in the SCS, respectively. The $NO_3^- + NO_2^-$ concentration at depths of less than 600 m in the SCS exceeds that in the WPS for two reasons. First, many rivers that are rich in NO_3^- and NO_2^- flow into the SCS. In particular, two of the largest rivers in the world (the Mekong and Pearl Rivers) enter from the north, contributing large amounts of nutrients and organic matter to the SCS, especially in the wet season (Yin et al., 2000; Chen et al., 2008). Also, the high-nutrient riverine water fuels higher productivity in the SCS relative to the WPS. Fig. 7 shows that the chlorophyll *a* concentrations in the surface and subsurface waters of the SCS are much higher than in the WPS, which reflects the higher productivity in the SCS.

Second, the deep WPS water flows across the deep sill (2200 m; Chen et al., 2001) into the SCS. This deep WPS water at around 2200 m becomes the deep water and the bottom water of the SCS (Nitani, 1972; Liu and Liu, 1988; Chen et al., 2001). The $NO_3^- + NO_2^-$ accumulates in the SCS, because of the flow pattern. This effect, together with the vertical mixing and upwelling, brings $NO_3^- + NO_2^-$ to the upper water, causing the concentration of $NO_3^- + NO_2^-$ in the SCS to be higher than that in the WPS at depths of less than 600 m, but lower at depths of greater than 600 m.

The vertical profiles of N_2O and DO and, in particular, the co-inciding N_2O maxima and DO minima (at 800–1000 m in the WPS and 600–800 m in the SCS), reveal that nitrification dominates the N_2O production, as was also found in previous research (Yoshinari, 1976). In short, the SCS has shallower N_2O maxima and DO minima than the WPS because of the intensive upwelling.

4.4. In situ biological production

Most studies in the field have used the contemporary atmospheric N_2O mole fraction, which is independent of the "real" age of the sampled water masses for the calculation of ΔN_2O. This approach is highly suitable for calculating ΔN_2O in waters in surface layers, but neglects the effect of the age of the water mass and, therefore, the variable atmospheric mole fraction that is involved in establishing an initial "equilibrium" (Walter et al., 2006; Freing et al., 2009). Nevison et al. (2003) asserted that the use of only the contemporary atmospheric mole fraction introduces an uncertainty of 10–15% in the estimate of ΔN_2O. Walter et al., (2006) showed that using "the contemporary atmospheric mole fraction" instead of "the initial atmospheric mole fraction" yielded a 7% smaller ΔN_2O at depths of less than 2000 m, and a 17% smaller ΔN_2O at depths of greater than 2000 m in the North Atlantic Ocean. This ΔN_2O difference at a particular depth may be higher in the Pacific Ocean than in the Atlantic Ocean because the deep water masses in the Pacific Ocean are older (England, 1995; Gebbie and Huybers, 2012). Fig. 8 presents the effect of depth-dependent initial atmospheric mole fractions on the ΔN_2O. There is no difference between the results above 350 m because the initial atmospheric mole fraction is taken to be equal to the contemporary atmospheric mole fraction. On the other hand, the equilibrium concentration of N_2O below 350 m that is calculated using the method herein, is generally lower than those obtained using a uniform N_2O mole fraction because "the initial atmospheric N_2O mole fraction" is lower than "the contemporary atmospheric N_2O mole fraction." Thus, the ΔN_2O may be underestimated by using a uniform atmospheric N_2O mole fraction. Therefore, we calculated the ΔN_2O herein by using different atmospheric N_2O
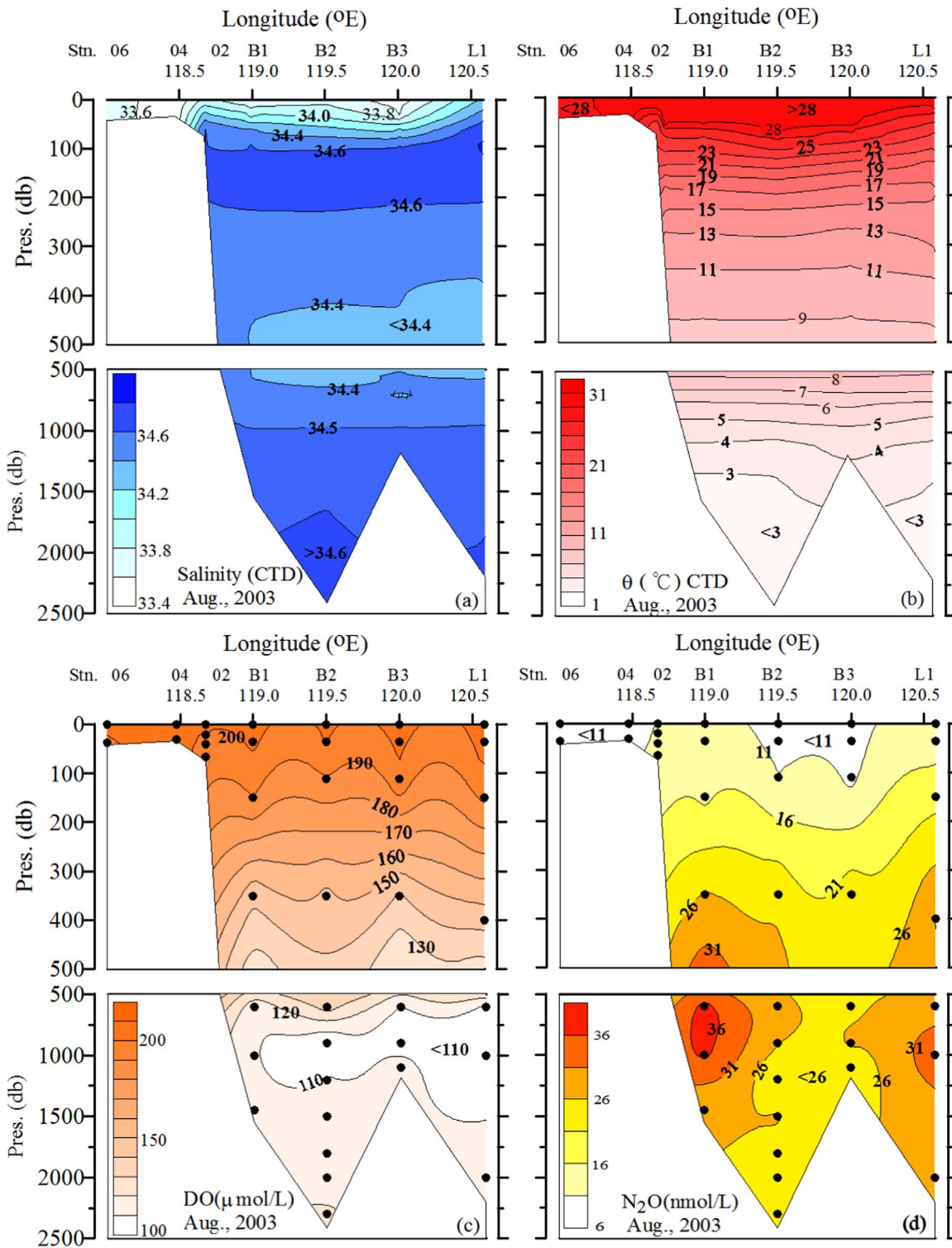
Fig. 4. Cross-section of (a) salinity; (b) potential temperature θ(°C); (c) DO (μmol L^{-1}); (d) N$_2$O (nmol L^{-1}) in the northeastern South China Sea, obtained at 7 stations during ORIII-896 cruise in August 2003.

mole fractions for different water layers to reduce the uncertainty of the ΔN$_2$O. Note there is a discontinuity in the percentage deviation of ΔN$_2$O at 350 m. This is caused by the sudden change of the initial atmospheric mole fraction from 318 to 321 ppb for waters above 350 m to 270 ppb for waters below 350 m. This artifact cannot yet be resolved without the knowledge of the exact age and the corresponding atmospheric N$_2$O concentration for subsurface water masses.

The ΔN$_2$O deviations at around 400–600 m in the WPS are rather large, because waters there have lower N$_2$O concentrations compared with that in the deeper water. To calculate ΔN$_2$O by using "the contemporary atmospheric mole fraction" instead of "the initial atmospheric mole fraction" may cause an error as high as 19% of the ΔN$_2$O deviation, especially in the area which has low N$_2$O concentrations. The mean ΔN$_2$O deviation below the surface layer is about $-6.1 \pm 2.0\%$ (n=131) in the WPS and $-4.1 \pm 0.5\%$
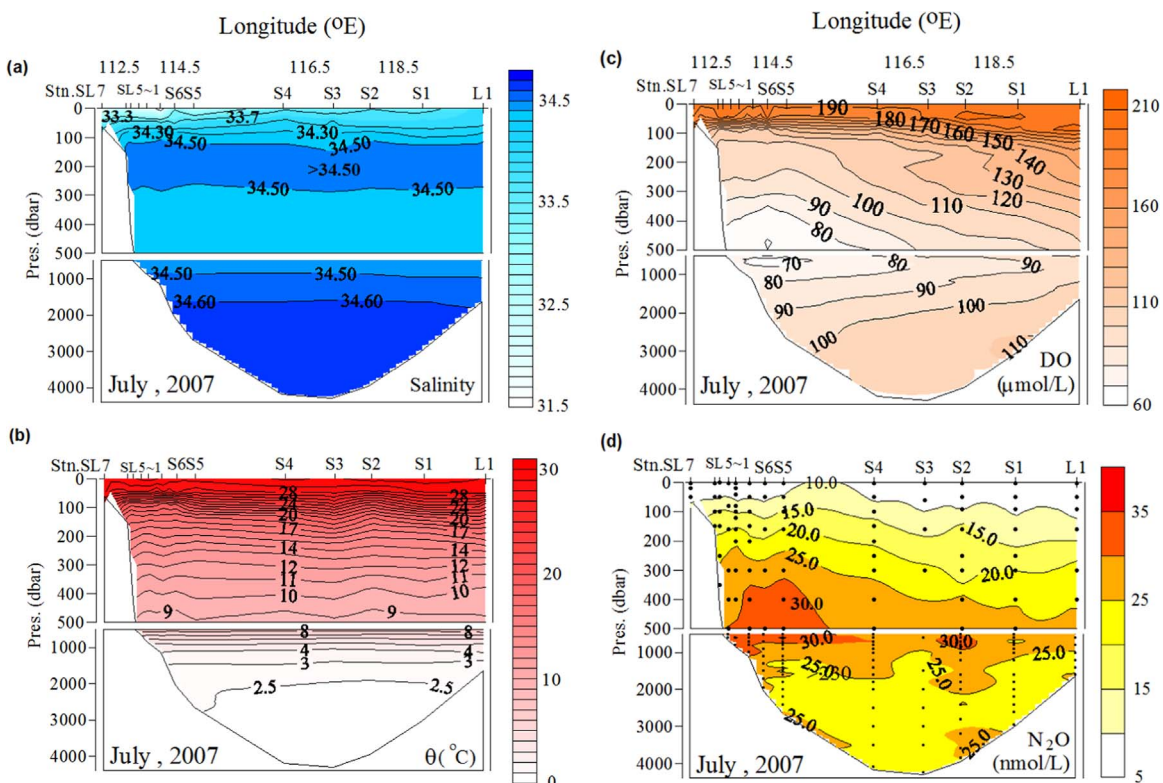
Fig. 5. Cross-section of (a) salinity; (b) potential temperature θ(°C); (c) DO (μmol L^{-1}); (d) N$_2$O (nmol L^{-1}) between the eastern and southern South China Sea, obtained at 13 stations during ORI-837 cruise in July 2007.

(n=234) in the SCS.

Several investigations have reported linear relationships between ΔN_2O and AOU in various oceanic areas (Yoshinari, 1976; Elkins et al., 1978; Cohen and Gordon, 1979; Butler et al., 1989; Law and Owens, 1990; Oudot et al., 1990; Naqvi and Noronha, 1991; Naqvi et al., 1994; Nevison et al., 1995, 2003). The AOU quantifies the amount of O$_2$ that is consumed by the remineralization of organic matter and nitrification in a water parcel since its last contact with the atmosphere. A strong correlation between AOU and ΔN_2O in the oceans is frequently observed, providing circumstantial evidence that nitrification is the dominant mechanism of oceanic N$_2$O production (Yoshinari, 1976; Elkins et al., 1978; Cohen and Gordon, 1979; Butler et al., 1989; Patra et al., 1999; Nevison et al., 2003).
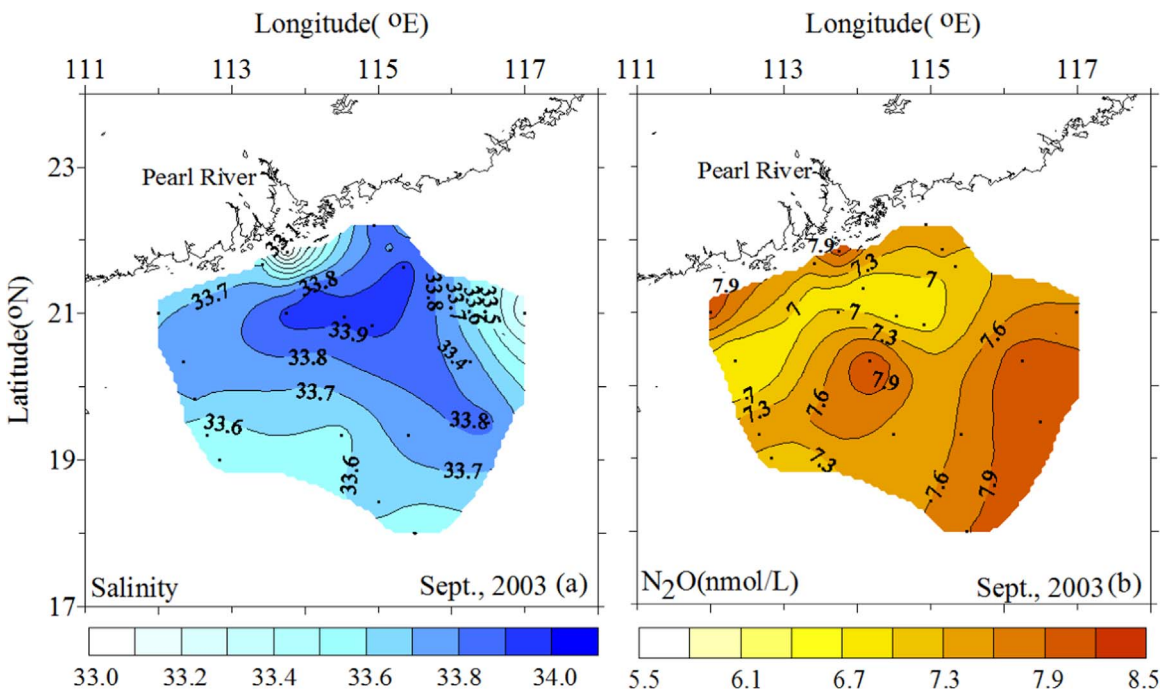

Fig. 6. Surface distributions of (a) salinity; (b) N$_2$O (nmol L^{-1}) near the Pearl River estuary, obtained at 22 stations during ORI-695 cruise in September 2003.
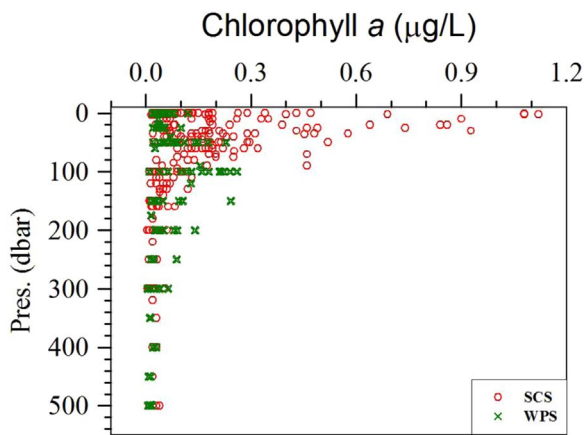
Fig. 7. Vertical distributions of chlorophyll *a* in the South China Sea and the West Philippines Sea above depth of 500 m, obtained at 91 stations during six cruises between August 2003 and July 2007.
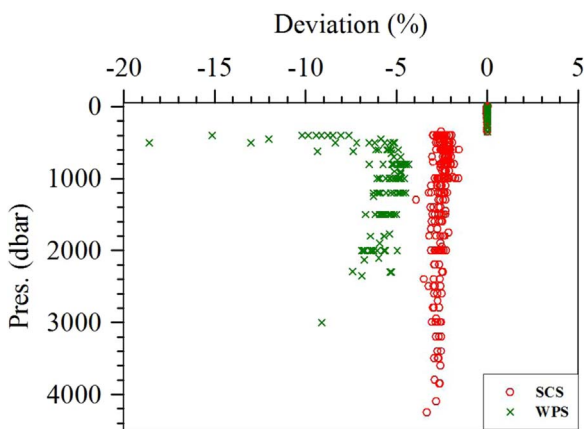

Fig. 8. The percentage deviation of ΔN_2O, between N_2O equilibrium concentration calculated using a uniform mole fraction of 318–321 ppb for years 2003–2007 and depth-dependent N_2O equilibrium concentration calculated using mole fractions of 318–321 ppb, 270 ppb and 260 ppb for the West Philippines Sea and mole fractions of 318–321 ppb and 270 ppb for the South China Sea.

Fig. 9. Comparison of ΔN_2O versus (a) AOU and (b) NO_3^- concentration in the West Philippines Sea and the South China Sea.

Fig. 9 reveals that at depths of less than that of the maximum N_2O concentrations (AOU $< 200\ \mu mol\ kg^{-1}$), ΔN_2O is positively correlated with AOU and NO_3^- in both the WPS and the SCS, implying that N_2O is produced mainly through biological processes. However, at depths that exceed that of the maximum N_2O concentration, ΔN_2O and AOU seem to be uncorrelated. In fact, ΔN_2O and NO_3^- even seem to be negatively correlated.

The relationships between ΔN_2O and AOU and between ΔN_2O and NO_3^- are studied to provide further insight into the biological production of N_2O. Horrigan et al. (1981) indicated that the production of N_2O is insignificant in the euphotic zone (from the surface to a depth of 15–100 m), where denitrifiers are inhibited by high oxygen concentrations and nitrifiers are inhibited by light and low NH_4^+ availability. To exclude the effects of sea-air exchange and photo-inhibition, the correlations between ΔN_2O and AOU (Fig. 10a) and between ΔN_2O and NO_3^- (Fig. 10b) from the lower euphotic zones (around 100 m) to the depth of the maximum N_2O concentration were examined. The ΔN_2O correlates positively with AOU (WPS: $\Delta N_2O = 0.091 AOU - 0.33$, n = 111, $r^2 = 0.96$; SCS: $\Delta N_2O = 0.121 AOU + 0.17$, n = 179, $r^2 = 0.87$) and NO_3^- (WPS: $\Delta N_2O = 0.53[NO_3^-] + 0.60$, n = 111, $r^2 = 0.94$; SCS: $\Delta N_2O = 0.70[NO_3^-] + 2.86$, n = 179, $r^2 = 0.88$), suggesting that nitrification is the major mechanism of the N_2O production at depths of less than 1000 m in the WPS and 800 m in the SCS. The slopes of the linear correlations between ΔN_2O and AOU provide
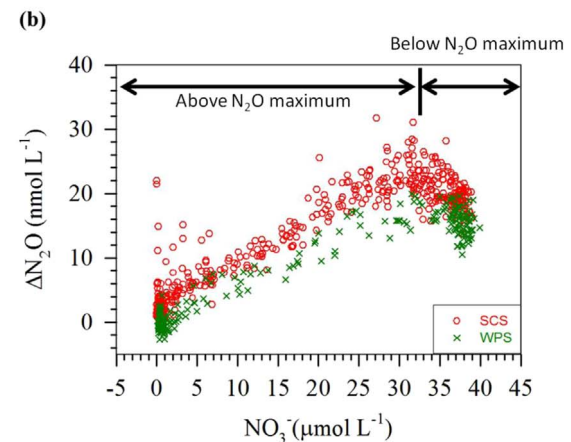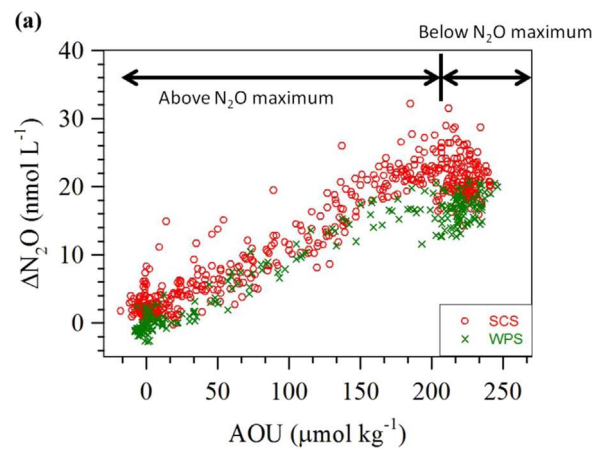
estimates of the amount of N_2O that is generated per amount of DO consumed (Nevison et al., 2003; Walker et al., 2010). N_2O yields from nitrification can be estimated from the DO consumption per mole of N_2O produced (Grundle et al., 2012), following the Redfield stoichiometry (Redfield et al., 1963), which attributes approximately 17.3% of the total DO consumption to the NH_4^+ oxidation (Ward, 2008). The correlations of ΔN_2O with AOU were utilized herein to reveal that the N_2O yield from nitrification was $0.053 \pm 0.001\%$ in the WPS and $0.070 \pm 0.002\%$ in the SCS between a depth of 100 m and that of the maximum N_2O concentration. Strong correlations between NO_3^- and AOU (Fig. 11c; WPS: $[NO_3^-] = 0.168[AOU] - 1.43$, n = 111, $r^2 = 0.98$; SCS: $[NO_3^-] = 0.167 [AOU] - 2.81$, n = 179, $r^2 = 0.91$) were also found, owing to nitrification in both the WPS and the SCS, as were also found in the western North Pacific (Yoshida et al., 1989). Hence, N_2O yields of nitrification could be estimated directly from the molar ratio of N_2O production to NO_3^- production, which was $0.053 \pm 0.001\%$ for the WPS and $0.070 \pm 0.002\%$ for the SCS from a depth of 100 m to the depth of the maximum N_2O concentration. These estimates match exactly those estimated from the relationship of ΔN_2O versus AOU. This finding supports that most of the N_2O in the subsurface water in the WPS and the SCS is produced by nitrification.

N_2O yield from nitrification in the SCS herein slightly exceeded 0.065% in the shelf region of the SCS (Han et al., 2013), and was also higher than the WPS. N_2O yields of nitrification in both the SCS and the WPS are higher than those reported elsewhere for the North Pacific Ocean (range, 0.004–0.027%; Yoshida et al., 1989), the NE subarctic Pacific Ocean (range, 0.028–0.040%; Grundle et al., 2012), and the subtropical Atlantic Ocean (0.030–0.040%; Walter
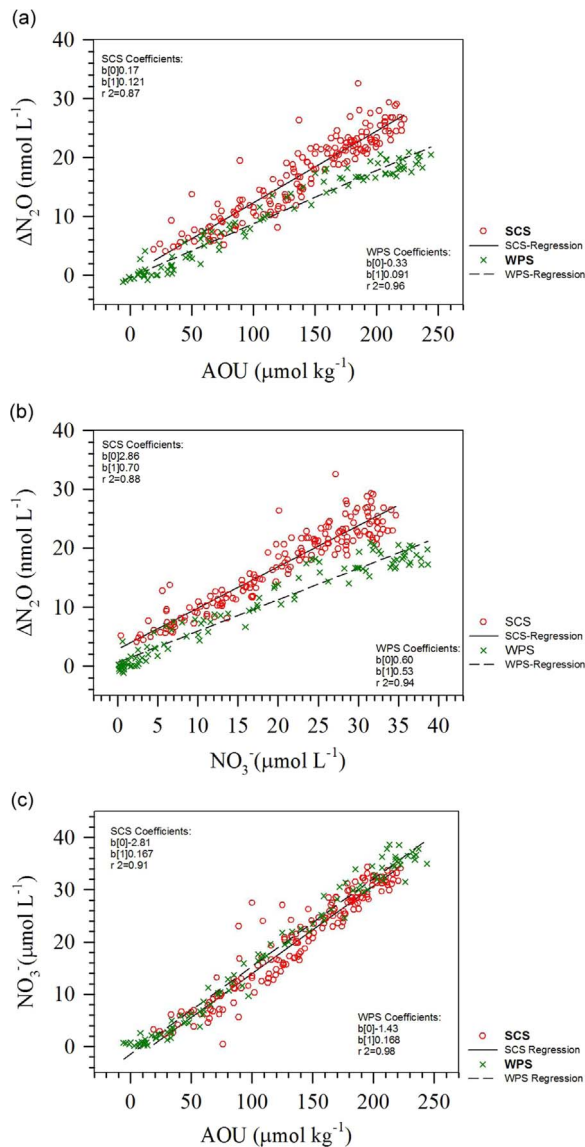
Fig. 10. Relationship between (a) ΔN_2O and AOU; (b) ΔN_2O and NO_3^- concentration; (c) NO_3^- concentration and AOU at between 100 m and depth of maximum N_2O concentration in the West Philippines Sea and the South China Sea.

et al., 2006), but are similar to those obtained for the tropical Atlantic Ocean (0.06–0.08%; Walter et al., 2006).

At depths greater than that of the maximum N_2O concentration, the linear relationships between ΔN_2O and AOU (Fig. 11a) as well as ΔN_2O and NO_3^- (Fig. 11b) in both the SCS and the WPS are statistically insignificant, presumably owing to changing N_2O yields and/or physical mixing of different water masses. Fig. 12 shows that the ΔN_2O/AOU ratios decrease with depth but remain constant below 1000 m both in the SCS and the WPS. Butler et al. (1989) hypothesized that the decline in the N_2O concentration with depth may reflect the pressure inhibition of the primary nitrification pathway that leads to the N_2O production. Nevison et al. (2003) and Codispoti (2010) also pointed out that the N_2O concentration and the ΔN_2O/AOU ratio tend to decrease at high pressure or AOU. The ΔN_2O concentrations and N_2O yields that are presented herein represent the N_2O production over the history of the water mass, rather than simply showing localized in situ production; since, the concentrations of preformed N_2O and the effects of conservative mixing were not eliminated (Nevison et al., 2003; Grundle et al., 2012).

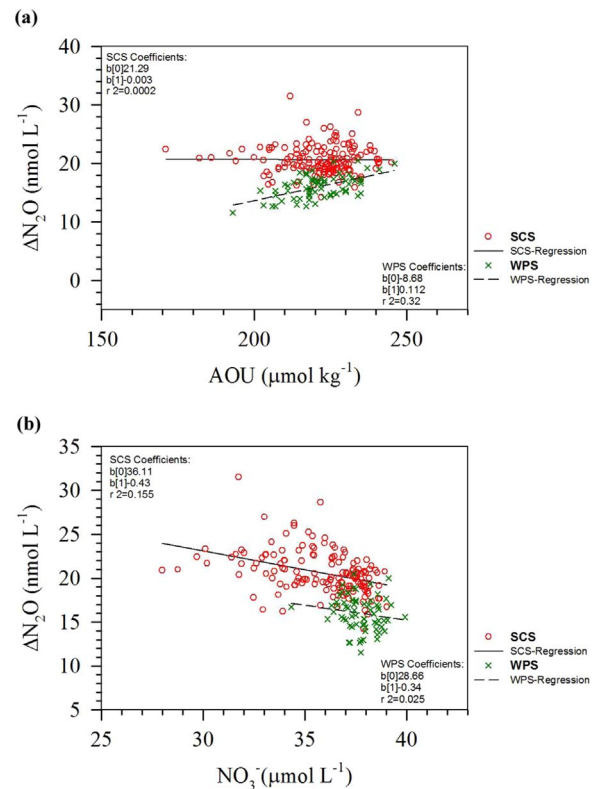In the WPS, the mean of the ΔN_2O/AOU ratio below the N_2O

maximum (800–1000 m) was 0.071 ± 0.008 (n=49), while the mean ΔN_2O/AOU ratio above the N_2O maximum was 0.091 ± 0.016 (n=86). In the SCS, the mean of the ΔN_2O/AOU ratio below the N_2O maximum (600–800 m) was 0.096 ± 0.013 (n=109), while the mean ΔN_2O/AOU ratio above the N_2O maximum was 0.118 ± 0.019 (n=180). In all, biological N_2O production per mole DO consumed in the SCS was around 23–26% higher than that in the WPS. This explains why N_2O distributions in the SCS were about 20% higher than that in the WPS.

The ΔN_2O/AOU ratios decreased at depths greater than that of the maximum N_2O concentration in the SCS, maybe because high pressure inhibited the primary nitrification pathway (Butler et al., 1989). However, since DO concentrations in the SCS deep water were at a relatively high level of around $100 \ \mu mol \ L^{-1}$,

Fig. 11. Relationship between (a) ΔN_2O and AOU; (b) ΔN_2O and NO_3^- concentration at depth greater than that of maximum N_2O concentration in the West Philippines Sea and the South China Sea.
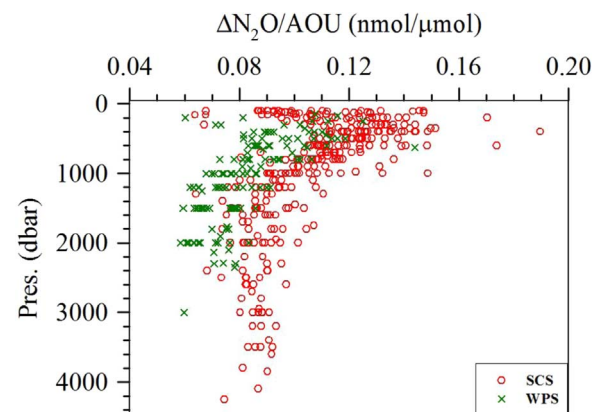

Fig. 12. Vertical distributions of ΔN_2O/AOU ratio in the South China Sea and the West Philippines Sea, obtained at 67 stations during seven cruises between August 2003 and July 2007.
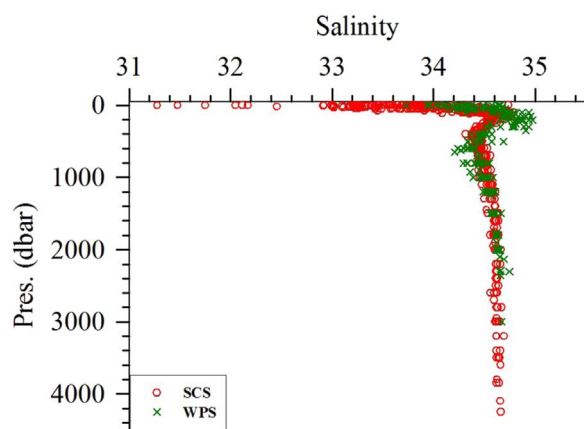
Fig. 13. Vertical distributions of salinity in the South China Sea and the West Philippines Sea, obtained at 114 stations during seven cruises between August 2003 and July 2007.

denitrification did not occur there. The N_2O concentrations decreased below the depth of the N_2O maximum in the SCS due to mixing with the WPS deep water, which has low N_2O concentrations. The N_2O concentration maximum in the SCS was about 28.85 nmol L^{-1} and the salinity was around 34.46 (Fig. 13) at depth of around 600–800 m. The N_2O concentration of the deep water layer (1350–2200 m) in the WPS was 20.43 nmol L^{-1} and the salinity was 34.62. The WPS deep water flows into the SCS and mixes with the SCS intermediate water, then becomes the SCS deep water with a salinity of 34.60. Calculation based on salinity indicates that the deep water of the SCS is composed of 88% WPS deep water and 12% SCS water at the N_2O maximum

($0.88 \times 34.62 + 0.12 \times 34.46$ $=34.60$). According to the water masses mixing ratio, 21.39 nmol L^{-1} of the N_2O concentration in the SCS deep water should have come from physical mixing ($0.88 \times 20.37 + 0.12 \times 28.85 = 21.39$). As a result, 85% of the N_2O concentration in the SCS deep water was from physical mixing and 15% was from biological N_2O production.

4.5. Air-sea N_2O exchange

During the wet season, the mean surface N_2O in the SCS was oversaturated and the sea-to-air flux was 5.5 ± 3.9 µmol m^{-2} d^{-1} (Table 2). The mean N_2O flux in the SCS during the wet season herein exceeds those from the shelf area of northwestern SCS (1.7 ± 1.6 µmol m^{-2} d^{-1}; Han et al., 2013) and those from the southern Baltic Sea (2.3–4.0 µmol m^{-2} d^{-1}; Bange et al., 1998). However, the flux in the SCS is comparable with or is only slightly lower than those from other seas – such as 9.8–17.1 µmol m^{-2} d^{-1} from the East China Sea (Zhang et al., 2008); 4.7–8.4 µmol m^{-2} d^{-1} from the North Yellow Sea (Yang et al., 2009); 5.2 µmol m^{-2} d^{-1} from the northwestern Black Sea (Amouroux et al., 2002), and 6.8–11.9 µmol m^{-2} d^{-1} from the north-eastern shelf of the Gulf of Cadiz (Ferrón et al., 2010). The SCS contributes about 0.1 Tg N to the atmosphere in the wet season which lasts for six months.

The mean surface N_2O concentration in the WPS in the wet season was undersaturated and the sea-to-air flux was -1.7 ± 3.9 µmol m^{-2} d^{-1} (Table 2). The WPS, the Golfe du Lion (Marty et al., 2001) and the Adriatic Sea (Leip, 1999) are a few of the marine areas for which N_2O undersaturations have been reported upon (Bange, 2006).

Table 2
Compilation of N_2O measurements in various coastal, shelf and marginal seas.

Study area	Date	Surface N_2O (nmol L^{-1})	Saturation (%)	Sea-to-Air Flux (µmol m^{-2} d^{-1})	Reference
NW Black Sea	Jul.–Aug. 1995	8.0 ± 0.8	110	3.1[a]; 5.2[b]	Amouroux et al., 2002
Caribbean Sea	June 1996	7.14 ± 0.21	120 ± 4	0.014 ± 0.014[a]	Morell et al., 2001
	Apr. 1995	6.60 ± 0.55	114 ± 9	0.069 ± 0.070[a]	
Arabian Sea	Sep.–Oct. 1986		187 ± 40	8.64 ± 4.32[a]	Law and Owens, 1990
	Apr. – May 1994		105 ± 8	0.06 ± 0.79[a]	Lal et al., 1996
	Feb. – Mar. 1995		132 ± 5	5.11 ± 4.12[a]	Lal and Patra, 1998
	Jul. – Aug. 1995		133 ± 15	10.01 ± 6.68[a]	
	Aug. 1996		130 ± 3	15.32 ± 7.66[a]	
Baltic sea	Aug. 1977–June 1980		123 (79–148)		Rönner, 1983
Southern Baltic Sea	June 1994–Apr. 1997		91–312	0.35–3.97[a] 0.60–7.08[b]	Bange et al., 1998
Aegean Sea	July 1993	7.02–7.27	103–107	1.2–21.0[a]	Bange et al., 1996b
Central North Sea and German Bight	Sep. 1991	8.4–9.2	99–104		Bange et al., 1996a
	Sep. 1992				
West Bay of Bengal	March–Apr. 1991		125.2 (89.3–214)	0.65[a] (−1.0–10.7)	Naqvi et al., 1994
Eastern Ionian Sea	Jul 1993		107 ± 3		Bange et al., 1996a
Gulf of Lions (Mediterranean Sea)	Jun 1998		86 (0–197)		Marty et al., 2001
Gulf of Thermaikos	Apr 1998		171 (84–309)		
Adriatic Sea	Aug 1996		93 (85–100)		Leip, 1999
NE shelf of the Gulf of Cadiz	Jun., Nov. 2006; Feb., May 2007	9.4–19.5	120–255	6.8 ± 6.4[a] 11.9 ± 10.6[b]	Ferrón et al., 2010
Tokyo Bay	May–Oct. 1994	9–139	116–1630	1.5–153[a]	Hashimoto et al., 1999
North Yellow Sea	Mar. 2005; Apr., Aug. 2006; Apr., Oct. 2007	12.0		4.7 ± 6.8[a] 8.4 ± 11.5[b]	Yang et al., 2009
East China Sea	Sep. 2003	11.5 ± 4.5 (5.75–24.1)	191 ± 74 (94–382)	9.8 ± 16.0[a] 17.1 ± 26.4[b]	Zhang et al., 2008
West Philippines Sea	Aug. 2004; May 2006; Jul. 2007	5.19 ± 1.26	90 ± 22	-1.7 ± 3.9[c]	This study
Northwestern South China Sea	Aug. 2008	5.51–7.74	99–123	1.1 ± 1.0[a] 1.7 ± 1.6[b]	Han et al., 2013
South China Sea	Aug., Sept., 2003; Jul. 2004; Jul. 2006; Jul. 2007	7.59 ± 1.32	132 ± 23	5.5 ± 3.9[c]	This study

Flux estimations are follows:

[a] Liss and Merlivat (1986);
[b] Wanninkhof (1992);
[c] Wanninkhof (2014).

Table 3
N$_2$O concentrations, water flux and N$_2$O flux of various water masses in the SCS and WPS.

	SCS			WPS		
	Avg. Concentration nmol L^{-1}	Water Flux $\times 10^6$ t s^{-1}	N$_2$O Flux $\times 10^6$ mol d^{-1}	Avg. Concentration nmol L^{-1}	Water Flux $\times 10^6$ t s^{-1}	N$_2$O Flux $\times 10^6$ mol d^{-1}
Surface Water Layer (0–350 m)	11.23 ± 5.17 (n=342)	−13.9 ± 1.8	−13.5	6.52 ± 2.82 (n=122)	12.8 ± 1.1	7.2
Intermediate water Layer (350–1350 m)	27.49 ± 2.88 (n=153)	−1.8 ± 0.4	−4.3			
Deep Water Layer (1350–2200 m)				20.37 ± 1.84 (n=36)	1.2 ± 0.2	2.1

Positive and negative numbers represent inflow and outflow, respectively.

4.6. Water mass and N$_2$O exchange between the SCS and the WPS

During the wet season, a net export of surface and intermediate waters from the SCS to the WPS occurs but there is a net import of deep water (Chen et al., 2001). The N$_2$O concentration at depths less than 350 m in the SCS (the SCS surface water layer) was 11.23 ± 5.17 nmol L^{-1}; that in the WPS (the WPS surface water layer) was 6.52 ± 2.82 nmol L^{-1} (Table 3). Chen et al. (2001) calculated the flow of surface water out of the SCS through the Bashi Channel during the wet season at 13.9 × 10^6 t s^{-1}, and the flow of WPS into the SCS at 12.8 × 10^6 t s^{-1}. Overall, the net exports of surface water from the SCS to the WPS carries 6.3 × 10^6 mol d^{-1} N$_2$O during the wet season.

The SCS intermediate water, as defined by Chen and Huang (1996) based on observational data, is at depths of between 350 and 1350 m, and is a mixture of the upwelled deep water and the surface water. The intermediate water flows out of the SCS at a rate of 1.8 × 10^6 t s^{-1} (Chao et al., 1996; Chen and Huang, 1996) with an N$_2$O concentration of 27.49 ± 2.88 nmol L^{-1}. Thus, the SCS intermediate water exports 4.3 × 10^6 mol d^{-1} N$_2$O to the WPS.

The deep water at depths of greater than 1350 m flows into the SCS year-round at a rate of 1.2 × 10^6 t s^{-1} (Chao et al., 1996; Chen and Huang, 1996). Since the deepest sill that connects the SCS with the WPS is 2200 m deep, water that is deeper than 2200 m cannot enter the SCS. The N$_2$O concentration of the deep water layer (1350–2200 m) in the WPS was 20.37 ± 1.84 nmol L^{-1}, so the deep water from the WPS exports 2.1 × 10^6 mol d^{-1} N$_2$O to the SCS.

Overall, in the wet season, the SCS exports 8.5 × 10^6 mol d^{-1} N$_2$O (net value) to the WPS and emits 19.3 × 10^6 mol d^{-1} N$_2$O to the atmosphere. Therefore, the SCS exports N$_2$O to the WPS and the atmosphere; and the SCS emits a larger amount of N$_2$O to the atmosphere than it transports to the WPS.

5. Conclusions

The surface waters are oversaturated in N$_2$O with respect to the atmosphere in the SCS, and undersaturated in the WPS. During the wet season, the SCS is a source of atmospheric N$_2$O at a rate of 5.5 ± 3.9 μmol m^{-2} d^{-1}, and the WPS is a sink of atmospheric N$_2$O at a rate of −1.7 ± 3.9 μmol m^{-2} d^{-1}.

The N$_2$O concentration in the water column in the SCS is higher than that in the WPS. The N$_2$O concentration in the WPS reached a maximum at a depth of 800–1000 m; the corresponding depth in the SCS was only around 600–800 m, owing to vertical mixing and intensive upwelling. Excess N$_2$O correlates positively with AOU and NO$_3^-$ suggesting that nitrification is the major mechanism of N$_2$O production at depths of less than 1000 m in the WPS and 800 m in the SCS. The N$_2$O yield from nitrification was 0.053% in the WPS and 0.070% in the SCS between a depth of 100 m and that of the maximum N$_2$O concentration, based on correlations of excess N$_2$O versus AOU and NO$_3^-$ concentrations. This study has established that the SCS emits N$_2$O to the atmosphere and exports N$_2$O to the WPS.

References

Amouroux, D., Roberts, G., Rapsomanikis, S., Andreae, M.O., 2002. Biogenic Gas (CH$_4$, N$_2$O, DMS) emission to the atmosphere from near-shore and shelf waters of the north-western Black Sea. Estuar. Coast. Shelf Sci. 54, 575–587.

Arévalo-Martínez, D.L., Kock, A., Löscher, C.R., Schmitz, R.A., Bange, H.W., 2015. Massive nitrous oxide emissions from the tropical South Pacific Ocean. Nat. Geosci. 8, 530–533.

Arp, D.J., Stein, L.Y., 2003. Metabolism of inorganic N compounds by ammonia-oxidizing bacteria. Crit. Rev. Biochem. Mol. Biol. 38, 471–495.

Bai, Y., Huang, T.H., He, X., Wang, S.L., Hsin, Y.C., Wu, C.R., Zhai, W., Lui, H.K., Chen, C.T.A., 2015. Intrusion of the Pearl River plume into the main channel of the Taiwan Strait in summer. J. Sea Res. 95, 1–15.

Bange, H.W., 2006. Nitrous oxide and methane in European coastal waters. Estuar. Coast. Shelf Sci. 70, 361–374.

Bange, H.W., 2008. Gaseous nitrogen compounds (NO, N$_2$O, N$_2$, NH$_3$) in the ocean. In: Caponeet et al., D.G. (Ed.), Nitrogen in the Marine Environment. Elsevier, pp. 55–93.

Bange, H.W., Andreae, M.O., 1999. Nitrous oxide in the deep waters of the world's oceans. Glob. Biogeochem. Cycles 13, 1127–1135.

Bange, H.W., Rapsomanikis, S., Andreae, M.O., 1996a. Nitrous oxide in coastal waters. Glob. Biogeochem. Cycles 10, 197–207.

Bange, H.W., Rapsomanikis, S., Andreae, M.O., 1996b. The Aegean Sea as a source of atmospheric nitrous oxide and methane. Mar. Chem. 53, 41–49.

Bange, H.W., Dahlke, S., Ramesh, R., Meyer-Reil, L.-A., Rapsomanikis, S., Andreae, M. O., 1998. Seasonal study of methane and nitrous oxide in the coastal waters of the Southern Baltic Sea. Estuar. Coast. Shelf Sci. 47 (6), 807–817.

Bange, H.W., Bell, T.G., Cornejo, M., Freing, A., Uher, G., Upstill-Goddard, R.C., Zhang, G., 2009. MEMENTO: a proposal to develop a database of marine nitrous oxide and methane measurements. Environ. Chem. 6, 195–197. http://dx.doi.org/10.1071/en09033.

Barnes, J., Owens, N.J.P., 1998. Denitrification and nitrous oxide concentrations in the Humber estuary, UK, and adjacent coastal zones. Mar. Pollut. Bull. 37 (3–7), 247–260.

de Bie, M.J.M., Middelburg, J.J., Starink, M., Laanbroek, H.J., 2002. Factors controlling nitrous oxide at the microbial community and estuarine scale. Mar. Ecol.: Prog. Ser. 240, 1–9.

Butler, J.H., Elkins, J.W., Thompson, T.M., 1989. Tropospheric and dissolved N$_2$O of the west Pacific and East Indian Oceans during the El Niño Southern Oscillation event of 1987. J. Geophys. Res. 94, 14865–14877.

Cao, Z.-M., Dai, M.-H., Zheng, N., Wang, D.-L., Li, Q., Zhai, W.-D., Meng, F.-F., Gan, J.-P., 2011. Dynamics of the carbonate system in a large continental shelf system under the influence of both a river plume and coastal upwelling. J. Geophys. Res. 116, G02010. http://dx.doi.org/10.1029/2010JG001596.

Capone, D.G., 1991. Aspects of the marine nitrogen cycle with relevance to the dynamics of nitrous and nitric oxide, in Microbial Production and Consumption of Greenhouse gases, edited by Rogers J.E., Whitman, W.E., pp. 255–275, Am. Soc. of Microbiol., Washington, D.C.

Chao, S.Y., Shaw, P.T., Wu, S.Y., 1996. Deep water ventilation in the South China Sea. Deep-Sea Res. 43, 445–466.

Chen, C.T., 1981. Oxygen solubility in seawater. In: Battino, R. (Ed.), Solubility Data Series vol. 7. Pergamon Press, Oxford, New York, Toronto, Sydney, Paris, Frankfurt, pp. 41–55.

Chen, C.T.A., Huang, M.H., 1995. Carbonate chemistry and the anthropogenic CO_2 in the South China Sea. Acta Oceanol. Sin. 14, 47–57.

Chen, C.T.A., Huang, M.H., 1996. A mid-depth front separating the South China Sea water and the West Philippine Sea water. J. Oceanogr. 52, 17–25.

Chen, C.T.A., Wang, S.L., Wang, B.J., Pai, S.C., 2001. Nutrient budgets for the South China Sea basin. Mar. Chem. 75, 281–300.

Chen, C.T.A., Hou, W.P., Gamo, T., Wang, S.L., 2006. Carbonate-related parameters of subsurface waters in the West Philippine, South China and Sulu Seas. Mar. Chem. 99, 151–161.

Chen, C.T.A., Yeh, Y.T., Chen, Y.C., Huang, T.H., 2015. Seasonal and ENSO-related interannual variability of subsurface fronts separating West Philippine Sea waters from South China Sea waters near the Luzon Strait. Deep-Sea Res. 103, 13–23.

Chen, C.T.A., Wang, S.L., Lu, X.X., Zhang, S.R., Lui, H.K., Tseng, H.C., Wang, B.J., Huang, H.I., 2008. Hydrogeochemistry and greenhouse gases of the Pearl River, its estuary and beyond. Quat. Int. 186, 79–90.

Codispoti, L.A., 2010. Interesting times for marine N_2O. Science 327 (5971), 1339–1340.

Codispoti, L.A., Yoshinari, T., Devol, A.H., 2005. Suboxic respiration in the oceanic water column. In: Del Giorgo, P.A., Williams, P.J.L.B. (Eds.), Respiration in Aquatic Ecosystems.. Oxford University Press, Oxford, pp. 225–247.

Cohen, Y., Gordon, L.I., 1979. Nitrous oxide production in the ocean. J. Geophys. Res. 84, 347–353.

Crutzen, P.J., 1970. The influence of nitrogen oxides on the atmospheric ozone content. Q. J. R. Meteorol. Soc. 96, 320–325.

Crutzen, P.J., 1974. Estimates of possible variations in total ozone due to natural causes and human activities. Ambio 3, 201–210.

Elkins, J.W., Wofsy, S.C., McElroy, M.B., Kolb, C.E., W. A, Kaplan, 1978. Aquatic sources and sinks for nitrous oxide. Nature 275, 602–6606.

England, M.H., 1995. The age of water and ventilation timescales a global ocean model. J. Phys. Oceanogr. 25, 2756–2777.

Ferrón, S., Ortega, T., Forja, J.M., 2010. Nitrous oxide distribution in the northeastern shelf of the Gulf of Cadiz (SW Iberian Peninsula). Mar. Chem. 119, 22–32.

Fluckiger, J., Dallenbach, A., Blunier, T., Stauffer, B., Stocker, T.F., Raynaud, D., Barnola, J.M., 1999. Variations in atmospheric N_2O concentration during abrupt climatic changes. Science 285 (5425), 227–230.

Freing, A., Wallace, D.W.R., Bange, H.W., 2012. Global oceanic production of nitrous oxide. Philos. Trans. R. Soc. B 367, 1245–1255.

Freing, A., Wallace, D.W.R., Tanhua, T., Walter, S., Bange, H.W., 2009. North Atlantic production of nitrous oxide in the context of changing atmospheric levels. Glob. Biogeochem. Cycles 23, GB4015. http://dx.doi.org/10.1029/2009GB003472.

Gan, J.-P., Li, L., Wang, D.-X., Guo, X.-G., 2009. Interaction of a river plume with coastal upwelling in the northeastern South China Sea. Cont. Shelf Res. 29, 728–740.

Gebbie, G., Huybers, P., 2012. The mean age of ocean waters inferred from radiocarbon observations: sensitivity to surface sources and accounting for mixing histories. J. Phys. Oceanogr. 42, 291–305.

Goreau, T.J., Kaplan, W.A., Wofsy, S.C., McElroy, M.B., Valois, F.W., Watson, S.W., 1980. Production of NO_2^- and N_2O by nitrifying bacteria at reduced concentrations of oxygen. Appl. Environ. Microbiol. 40, 526–532.

Gruber, N., Galloway, J.N., 2008. An earth-system perspective of the global nitrogen cycle. Nature 451, 293–296. http://dx.doi.org/10.1038/nature06592.

Grundle, D.S., Maranger, R., Juniper, S.K., 2012. Upper water column nitrous oxide distributions in the northeast subarctic Pacific ocean. Atmos. -Ocean 50 (4), 475–486.

Tseng, H.C., Chen, C.T.A, Borges, A.V., DelValls, T.A., Chang, Y.C., 2016. Methane distributions and sea-to-air fluxes in the South China Sea and the West Philippines Sea. Cont. Shelf Res., (submitted for publication).

Han, A.-Q., Dai, M.-H., Kao, S.-J., Gan, J.-P., Li, Q., Wang, L.-F., Zhai, W.-D., Wang, L., 2012. Nutrient dynamics and biological consumption in a large continental shelf system under the influence of both a river plume and coastal upwelling. Limnol. Oceanogr. 57, 486–502.

Han, W.-Y., 1998. Marine Chemistry in the South China Sea, Beijing. Science Press,, p. 289 (in Chinese).

Han, Y., Zhang, G.L., Zhao, Y.C., Liu, S.M., 2013. Distributions and sea-to-air fluxes of nitrous oxide in the coastal and shelf waters of the northwestern South China Sea. Estuar. Coast. Shelf Sci. 133, 32–44.

Hashimoto, S., Gojo, K., Hikota, S., Sendai, N., Otsuki, A, A, 1999. Nitrous oxide emissions from coastal waters in Tokyo Bay. Mar. Environ. Res. 47, 213–223.

Herbeck, L.S., Unger, D., Krumme, U., Liu, S.M., Jennerjahn, T.C., 2011. Typhoon-induced precipitation impact on nutrient and suspended matter dynamics of a tropical estuary affected by human activities in Hainan, China. Estuar. Coast. Shelf Sci. 93, 375–388.

Horrigan, S.G., Carlucci, A.F., Williams, P.M., 1981. Light inhibition of nitrification in sea-surface films. J. Mar. Res. 39 (3), 557–565.

Intergovernmental Panel on Climate Change (IPCC), 2013: Working Group I Report, The Physical Science Basis. C.2; C.6; C.8, pp. 159–254; pp.473 – 552; pp. 677–731.

Johnson, K.M., Hughes, J.E., Donaghay, P.L., Sieburth, J.M., 1990. Bottle-calibration static head space method for the determination of methane dissolved in seawater. Anal. Chem. 62, 2408–2412.

Lal, S., Patra, P.K., 1998. Variabilities in the fluxes and annual emissions of nitrous oxide fromtheArabian Sea. Glob. Biogeochem. Cycles 12 (2), 321–327.

Lal, S., Patra, P.K., Venkataramani, S., Sarin, M.M., 1996. Distribution of nitrous oxide and methane in the Arabian Sea. Curr. Sci. 71 (11), 894–899.

LaMontagne, M.G., Duran, R., Valiela, I., 2003. Nitrous oxide sources and sinks in coastal aquifers and coupled estuarine receiving waters. Sci. Total Environ. 309, 139–149.

Law, C.S., Owens, N.J.P., 1990. Significant flux of atmospheric nitrous oxide from the northwest Indian Ocean. Nature 346, 826–828.

Leip, A., 1999. Nitrous Oxide (N_2O) Emissions From a Coastal Catchment in The Delta of The Po River: Measurements and Modeling of Fluxes From a Mediterranean Lagoon And Agricultural Soils. University Of Bayreuth,, Bayreuth, Germany (unpublished).

Lin, S., Liu, K.K., Chen, M.P., Chen, P., Chang, F.Y., 1992. Distribution of organic carbon in the KEEP area continental margin sediments. Terr. Atmos. Ocean. Sci. 3 (3), 365–378.

Liss, P.S., Merlivat, L., 1986. Air-sea gas exchange rates: introduction and synthesis in the role of air-sea exchange in geochemical cyclings. Mass: D. Reide, Norwell, 113–1127.

Liu, C.T., Liu, R.J., 1988. The deep current in the Bashi Channel. Acta Oceanogr. Taiwan 20, 107–116.

MacFarling Meure, C., Etheridge, D., Trudinger, C., Steele, P., Langenfelds, R., van Ommen, T., Smith, A., Elkins, J., 2006. Law Dome CO_2, CH_4 and N_2O ice core records extended to 2000 years BP. Geophys. Res. Lett. 33. http://dx.doi.org/10.1029/2006GL026152.

Manizza, M., Keeling, R., Nevison, C.D., 2012. On the processes controlling the seasonal cycles of the air-sea fluxes of O_2 and N_2O: A modelling study. Tellus B 64, 18429.

Marty, D., Bonin, P., Michotey, V., Bianchi, M., 2001. Bacterial biogas production in coastal systems affected by freshwater inputs. Cont. Shelf Res. 21, 2105–2115.

Middelburg, J.J., Soetaert, K., Herman, P.M.J., Heip, C.H.R., 1996. Denitrification in marine sediments: a model study. Glob. Biogeochem. Cycles 10 (4), 661–673.

Morell, J.M., Capella, J., Mercado, A., Bauza, J., Corredor, J.E., 2001. Nitrous oxide fluxes in Caribbean and tropical Atlantic waters: evidence for near surface production. Mar. Chem. 74, 131–143.

Myhre, G., Shindell, D., Bréon, F.-M., Collins, W., Fuglestvedt, J., Huang, J., Koch, D., Lamarque, J.-F., Lee, D., Mendoza, B., Nakajima, T., Robock, A., Stephens, G., Takemura, T., Zhang, H., 2013: Anthropogenic and natural radiative forcing, in: Climate Change 2013: The Physical Science Basis. Contribution of Working Group I to the Fifth Assessment Report of the Intergovernmental Panel on Climate Change.

Naik, H., Naqvi, S.W.A., Suresh, T., Narvekar, P.V., 2008. Impact of a tropical cyclone on biogeochemistry of the central Arabian Sea. Glob. Biogeochem. Cycles 22, GB3020.

Najjar, R.G., 1992. Marine biogeochemistry. In: Trenberth, K.E. (Ed.), Climate System Modeling. Cambridge University Press, New York, pp. 241–280.

Naqvi, S.W.A., Noronha, R.J., 1991. Nitrous oxide in the Arabian Sea. Deep-Sea Res. 38, 871–890.

Naqvi, S.W.A., Jayakumar, D.A., Nair, M., Kumar, M.D., George, M.D., 1994. Nitrous oxide in the western Bay of Bengal. Mar. Chem. 47, 269–278.

Naqvi, S.W.A., Bange, H.W., Farías, L., Monteiro, P.M.S., Scranton, M.I., Zhang, J., 2010. Marine hypoxia/anoxia as a source of CH_4 and N_2O. Biogeosciences 7, 2159–2190.

Naqvi, S.W.A., Yoshinari, T., Jayakumar1, D.A., Altabet, M.A., Narvekar1, P.V., Devol, A.H., Brandes, J.A., Codispoti, L.A., 1998. Budgetary and biogeochemical implications of N_2O isotope signatures in the Arabian Sea. Nature 394, 462–4464.

Nevison, C., Butler, J.H., Elkins, J.W., 2003. Global distributions of N_2O and ΔN_2O–AOU yield in the subsurface ocean. Glob. Biogeochem. Cycles 18, GB1018.

Nevison, C.D., Holland, E.A., 1997. A reexamination of the impact of anthropogenically fixed nitrogen on atmospheric N_2O and the stratospheric O_3 layer. J. Geophys. Res. 102 (25) 519–25,536, 1997.

Nevison, C.D., Weiss, R.F., Erickson III, D.J., 1995. Global oceanic emissions of nitrous oxide. J. Geophys. Res. 100, 15809–15820.

Nitani, H., 1972. Beginning of the Kuroshio. p. 129–163. In: Stommel, H., Yoshida, K. (Eds.), Kuroshio. Univ. Washington Press.

Oudot, C., Andrie, C., Montel, Y., 1990. Nitrous oxide production in the tropical Atlantic Ocean. Deep-Sea Res. 37, 183–202.

Pai, S.-C., Yang, C.-C., Riley, J.P., 1990. Formation kinetics of the pink azo dye in the determination of nitrate in natural waters. Anal. Chim. Acta 232, 345–349.

Pai, S.-C., Gong, G.-C., Liu, K.-K., 1993. Determination of dissolved oxygen in seawater by direct spectrophotometry of total iodine. Mar. Chem. 41, 343–351.

Patra, P.K., Lal, S., Venkataramani, S., de Sousa, S.N., Sarma, V.V.S.S., Sardesai, S., 1999. Seasonal and spatial variability in N_2O distribution in the Arabian Sea. Deep-Sea Res. Part I 46, 529–543.

Prather, M., et al., 2001. Atmospheric chemistry and greenhouse gases, in Climate Change 2001: the Scientific Basis: Contribution of Working Group I to the Third. In: Houghton, J.T., et al. (Eds.), Assessment Report of the Intergovernmental Panel on Climate Change. Cambridge Univ. Press, New York, pp. 239–287.

Prather, M.J., Holmes, C.D., Hsu, J., 2012. Reactive greenhouse gas scenarios: systematic exploration of uncertainties and the role of atmospheric chemistry. Geophys. Res. Lett. 39, L09803. http://dx.doi.org/10.1029/2012gl051440.

Rönner, U., 1983. Distribution, production and consumption of N_2O in the Baltic Sea. Geochim. Cosmochim. Acta 47, 2179–2188.

Ravishankara, A.R., Daniel, J.S., Portmann, R.W., 2009. Nitrous oxide (N_2O): the dominant ozone-depleting substance emitted in the 21st Century. Science 326 (5949), 123–125.

Redfield, A.C., Ketchum, B.H., Richards, F.A., 1963. The influence of organisms on the composition of sea water. In: Hill (Ed.), The Sea Vol 2. Wiley Inter Science, New York, pp. 26–77.

Robinson, A.D., Nedwell, D.B., Harrison, R.M., Ogilvie, B.G., 1998. Hypernutrified estuaries as sources of N_2O emission to the atmosphere: the estuary of the River Colne, Essex, UK. Mar. Ecol. Prog. Ser. 164, 59–71.

Saikawa, E., Prinn1, R.G., Dlugokencky, E., Ishijima, K., Dutton, G.S., Hall, B.D., Langenfelds, R., Tohjima, Y., Machida, T., Manizza, M., Rigby, M., O'Doherty, S., Patra, P.K., Harth, C.M., Weiss, R.F., Krummel, P.B., van der Schoot, M., Fraser, P.J., Steele, L.P., Aoki, S., Nakazawa, T., Elkins, J.W., 2014. Global and regional emissions estimates for N_2O. Atmos. Chem. Phys. 14, 4617–4641.

Seitzinger, S.P., 1988. Denitrification in freshwater and coastal marine ecosystem: Ecological and geochemical significance. Limnol. Oceanogr. 33, 702–724.

Stein, L.Y., Yung, Y.L., 2003. Production, isotopic composition, and atmospheric fate of biologically produced nitrous oxide. Ann. Rev. Earth Planet. Sci. 31, 329–356.

Strickland, J.D.H., Parsons, T.R., 1972. A Practical Handbook of Seawater Analysis. Fisheries Research Board Of Canada,, , Ottawa, Canada, p. 310.

Suntharalingam, P., Sarmiento, J.L., 2000. Factors governing the oceanic nitrous oxide distribution: simulations with an ocean general circulation model. Glob. Biogeochem. Cycles 14, 429–454. http://dx.doi.org/10.1029/1999gb900032.

Usui, T., Koike, I., Ogura, N., 1998. Vertical profiles of nitrous oxide and dissolved oxygen in marine sediment. Mar. Chem. 59, 253–2270.

Usui, T., Koike, I., Ogura, N., 2001. N_2O Production, nitrification and denitrification in an estuarine sediment. Estuar. Coast. Shelf Sci. 52, 769–781.

Walker, J.T., Stow, C., Geron, C., 2010. Nitrous oxide emissions from the Gulf of Mexico hypoxic zone. Environ. Sci. Technol. 44, 1617–1623.

Walsh, J.J., Premuzic, E.T., Gaffney, J.S., Rowe, G.T., Harbottle, G., Stoenner, R.W., Balsam, W.L., Betzer, P.R., Macko, S.A., 1985. Organic storage of CO_2 on the continental slope off the mid-Atlantic bight, the southeastern Bering Sea, and the Peru coast. Deep Sea Res. 32, 853–883.

Walter, S., Bange, H.W., Breitenbach, U., Wallace, D.W.R., 2006. Nitrous oxide in the North Atlantic Ocean. Biogeosciences 3 (4), 607–619.

Wanninkhof, R., 1992. Relationship between wind speed and gas exchange over the ocean. J. Geophys. Res. 97 (C5), 7373–7382.

Wanninkhof, R., 2014. Relationship between wind speed and gas exchange over the ocean revisited. Limnol. Oceanogr.: Methods 12, 351–362.

Ward, B.B., 2008. Nitrification in marine systems. In: Capone, D.G., Bronk, D.A., Mullholand, M.R., Carpenter, E.J. (Eds.), Nitrogen in the Marine Environment, second ed. Academic Press, Burlington, MA, pp. 199–262.

Ward, B.B., Glover, H.E., Lipschultz, F., 1989. Chemoautotrophic activity of nitrification in the oxygen minimum zone off Peru. Deep Sea Res. 36, 1031–1051.

Weiss, R.F., Price, B.A., 1980. Nitrous oxide solubility in water and seawater. Mar. Chem. 8, 347–359.

Wrage, N., Velthof, G.L., Van Beusichem, M.L., Oenema, O., 2001. Role of nitrifier denitrification in the production of nitrous oxide. Soil. Biol. Biochem. 33, 1723–1732.

Xu, J.R., Wang, Y.S., Yin, J.P., Wang, Q.J., Zhang, F.Q., He, L., Sun, C.-C., 2006. Transformation of dissolved inorganic nitrogen species and nitrification and denitrification processes in the near sea section of Zhujiang River. Acta Sci. Circumst. 25, 686–692 (in Chinese).

Yang, J., Zhang, G.L., Zheng, L.X., Zhang, F., 2009. Seasonal variations of fluxes and distributions of dissolved N_2O in the north yellow sea. Environ. Sci. 30 (3), 656–662 (in Chinese).

Yin, K., Qian, P., Chen, Jv.C., Hsieh, D.P.H., Harrison, P.J., 2000. Dynamics of nutrients and phytoplankton biomass in the Pearl River estuary and adjacent waters of Hong Kong during summer: preliminary evidence for phosphorus and silicon limitation. Mar. Ecol.: Prog. Ser. 194, 295–305.

Yin, K.D., Zhang, J.L., Qian, P.Y., Jian, W.J., Huang, L.M., Chen, J.F., Wu, M.C.S., 2004. Effect of wind events on phytoplankton blooms in the Pearl River estuary during summer. Cont. Shelf Res. 24, 1909–1923.

Yoshida, N., Morimoto, H., Hirano, M., Koike, I., Matsuo, S., Wada, E., Saino, T., Hattori, A., 1989. Nitrification rates and 15N abundances of N_2O and NO_3^- in the western North Pacific. Nature 342, 895–897.

Yoshinari, T., 1976. Nitrous oxide in the sea. Mar. Chem. 4, 189–202.

Zamora, L.M., Oschlies, A., Bange, H.W., Huebert, K.B., Craig, J.D., Kock, A., Löscher, C. R., 2012. Nitrous oxide dynamics in low oxygen regions of the Pacific: insights from the MEMENTO database. Biogeosciences 9, 5007–5022. http://dx.doi.org/10.5194/bg-9-5007–2012.

Zehr, J.P., Ward, B.B., 2002. Nitrogen cycling in the ocean: new perspectives on processes and paradigms. Appl. Environ. Micro. 68, 1015–1024. http://dx.doi.org/10.1128/aem.68.3.1015–1024.2002.

Zhai, W.-D., Dai, M.-H., Chen, B.-S., Guo1, X.-H., Li, Q., Shang, S.-L., Zhang, C.-Y., Cai, W.-J., Wang, D.-X., 2013. Seasonal variations of sea–air CO_2 fluxes in the largest tropical marginal sea (South China Sea) based on multiple-year underway measurements. Biogeosciences 10, 7775–7791.

Zhang, G.L., Zhang, J., Ren, J.L., Li, J.B., Liu, S.M., 2008. Distributions and sea-to-air fluxes of methane and nitrous oxide in the North East China Sea in summer. Mar. Chem. 110 (1–2), 42–455.

Zheng, G.M., Tang, D.L., 2007. Offshore and nearshore chlorophyll increases induced by typhoon winds and subsequent terrestrial rainwater runoff. Mar. Ecol.: Prog. Ser. 333, 61–74.

Zheng, L.X., Zhang, G.L., Xu, J., Zhang, F., Zhang, J., 2009. Distribution and air-sea fluxes of N_2O in South China Sea in spring. Mar. Environ. Sci. 28 (3), 233–2237 (in Chinese).

Zhu, Z.Y., Zhang, J., Wu, Y., Lin, J., 2006. Bulk particulate organic carbon in the East China Sea: tidal influence and bottom transport. Prog. Oceanogr. 69, 37–60.